Strain measurements using Fiber Bragg Grating sensors in Structural Health Monitoring

Daniela ENCIU*,[1], Mihai TUDOSE[1], Camelia Elena MUNTEANU[1], Ioan URSU[1]

*Corresponding author
[1]INCAS − National Institute for Aerospace Research "Elie Carafoli",
220 Blvd. Iuliu Maniu, Bucharest 061126, Romania,
enciu.daniela@incas.ro*, tudose.mihai@incas.ro, munteanu.camelia@incas.ro,
ursu.ioan@incas.ro

DOI: 10.13111/2066-8201.2017.9.2.6

Received: 30 April 2017/ Accepted: 25 May 2017/ Published: June 2017

Abstract: *The paper presents some results obtained within a project of the "NUCLEU" Program financed by the Ministry of Research and Innovation-ANCS. The project supposes, among others, the design and the realization of a demonstrator for strain and stress measurements made with Fiber Bragg Gratings optical sensors. The paper details the construction of the demonstrator. The strain measurements induced in a cantilevered aluminum plate are compared with the analytical values provided by a mathematical model, and with the numerical values obtained by FEM analysis. The consistency of these comparative data indicates the achievement within the project of a level of competence necessary for later use of FBG sensors in the applicative researches involving the aerospace structures monitoring.*

Key Words: *Fiber Bragg Gratings, plate bending, strain measurement, Structural Health Monitoring*

1. INTRODUCTION

The electric sensors have been for many years the standard instruments for measuring the physical and dynamic parameters of the mechanisms, structures, phenomena, etc. But interference with the electromagnetic field has led to the search for another type of sensors.

The most suitable sensors with such requirement are Bragg optical fibers. Innovations in the optoelectronic field over the last twenty years have led to a considerable reduction in the cost of such a sensor and to the improvement of its quality and of the information transmitted through the fiber.

For this reason, fiber-based sensors have moved from laboratory research to wide-use applications. One of the applications is to monitor the health of the structures [1]-[6].

The main structure of an optical fiber is: core, coating, protective coating (Fig. 1a). The coating reflects the light beams back into the core of the fiber, ensuring the transmission of light through the entire fiber with minimal loss of information.

A high refractive index of the fiber core compared to the coating index provides a total internal reflection of the light. The protective layer helps to protect the fiber from external conditions and physical defects [3]. Depending on the fiber destination, different coatings can be added to the applications to be used. The most widely used optic sensor is optical Fiber Bragg Gratings (FBG) sensor [5], [7]. Optical fiber works on the principle of

modulation of wave propagation, intensity, phase, polarization, frequency, in response to measured parameters [8]. Extrinsic optical sensors use fiber only to transmit light to and from a sensor, while intrinsic optical sensors use the fiber itself as the sensor itself. The wavelength of light varies with changes in temperature and/or deformation [9], [10].

Since FBGs respond to both deformations and temperature, both effects have to be considered and a way to distinguish between must be found. In the case of the temperature sensor, the FBG must remain undeformed, not be coupled to bending, torsion, traction, compression forces. To ensure that the sensor remains undeformed, FBG sensors are used in certain protective layers. Thus, the deformation measurements will be processed by applying a method of compensating the temperature effects on the FBG.

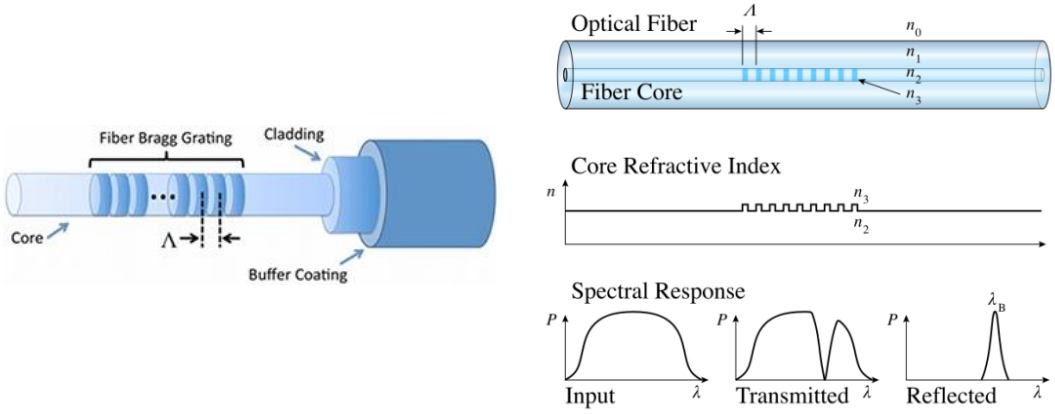

Fig. 1 (a) The structure of an optical fiber bragg grating sensor (http://www.ni.com/white-paper/11821/en/); (b) the refractive index profile and spectral response (see https://en.wikipedia.org/wiki/Fiber_Bragg_grating)

The principle of operating of the optical fiber with FBG, described briefly, is the following: a laser beam is transmitted through the fiber. Part of the light will be reflected, that of length λ_B, the other one will be transmitted (Fig. 1b).

Current technologies for monitoring the state of health of structures are increasingly dependent on optical sensors. In an ongoing project funded by the Ministry of Research and Innovation – ANCS, Program "NUCLEU", a demonstrator was carried out on the use of optical FBG sensors in high precision measurements of physical, mechanical and dynamic parameters. In fact, the know-how of these measurements is a mandatory preamble to defect detection methodology. The demonstrator contains the following basic components: 1) the specimen (an aluminum plate), 2) an actuator which generates precisely controlled movements of the plate and whose precision is also proven by movement measurements with a laser sensor, 3) software and 4) optic and recording equipment.

2. ELEMENTS OF ANALYTICAL AND NUMERICAL MODELLING AND MEASURING WITH FBG OF INDUCED STRAIN IN A CANTILEVERED ALUMINUM PLATE

The sketch on Fig. 2 is well known in literature (e.g. [11]). A FBG optical sensor is bonded on the plate at the distance x from the fixed (embedded) end. The ultimate objective is to determine the strain at different position of the sensor. The differential equation for the deflection curve $v(x)$ of the "middle elastic line" of the rectangular plate, when a force F is applied at its free end is

$$\frac{d^2v}{dx^2} = -\frac{M}{EI_z} \tag{1}$$

where M is the bending moment, E is the modulus of elasticity of the material, and I is the moment of inertia of the plate in direction z of bending; l and g are the width and the thickness of the plate

$$M = -F(L - x)$$

$$I_z = \frac{1}{12} l g^3$$

Then equation (1) becomes

$$\frac{d^2v}{dx^2} = \frac{12F(L - x)}{Elg^3} \tag{2}$$

The angle of rotation φ of the plate middle line, at the level x where the FBG "center" is located, is thus written

$$\varphi = \frac{dv}{dx} = \frac{12F}{Elg^3}\left(Lx - \frac{x^2}{2}\right) + C_1$$

and the deflection is

$$v = \frac{12F}{Elg^3}\left(L\frac{x^2}{2} - \frac{x^3}{6}\right) + xC_1 + C_2$$

From the boundary conditions of the plate, $\varphi(x) = 0$, and $v(x) = 0$, for $x = 0$, then the values of the constants C_1 si C_2 are determined: $C_1 = 0$, $C_2 = 0$. The angle of rotation and the deflection will be

$$\varphi = \frac{6F}{Elg^3} x(2L - x) \tag{3}$$

$$v = \frac{2F}{Elg^3} x^2(3L - x) \tag{4}$$

For the case when $x = L$, the maximum values will be

$$\varphi_{max} = \frac{6FL^2}{Elg^3} \tag{3'}$$

$$v_{max} = \frac{4FL^3}{Elg^3} \tag{4'}$$

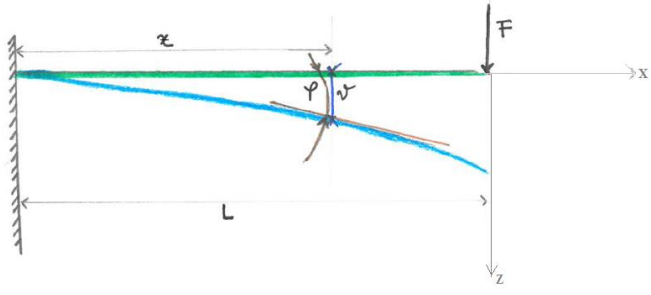

Fig. 2 Sketch of the cantilevered aluminum plate

At this point, classic hypotheses are recalled. "Bernoulli assumes that each plane cross-section of the beam remains plane also after bending. Navier concludes from this that the normal stresses transmitted by a cross-section are distributed according to a *linear law*" [12], p. 294. In the present case, Navier's law is thus formulated

$$\sigma = -\frac{My}{I_z} \tag{5}$$

where y is the distance from the surface of the plate to the middle line. Then, from Hooke's law of linear relation between stress and strain (valid if the loads are assumed to be small enough, [12], pp. 61-62).

$$\sigma = E\varepsilon \tag{6}$$

the strain can be deduced from the following relation

$$\varepsilon = \frac{6F(L-x)}{Elg^2} \tag{7}$$

or it can be expressed as a relation involving the maximum deflection

$$\varepsilon = \frac{3gv_{max}(L-x)}{2L^3} \tag{8}$$

Below are some basic elements of strain measurement using FBG [13]. The gratings for an unstrained FBG (Fig. 2) have a specific distance between them, Λ, given by:

$$\Lambda = \frac{\lambda_0}{2n} \tag{9}$$

where λ_0 is the wavelength of the peak, and n the refractive index. When the fiber is subjected to mechanical deformations, the distance of the grids is also modified making changes in the reflected and transmitted wavelength.

An FBG sensor is sensitive to both strain and temperature, therefore the wavelength is changing according to the relation

$$\frac{\Delta\lambda}{\lambda_0} = K \cdot \varepsilon + a_g \cdot \Delta T \tag{10}$$

with $\Delta\lambda = \lambda - \lambda_0$, where λ is the current wavelength of the optical sensor, and λ_0 the reference wavelength of the strain gauge. K is the sensor gage factor, $K = 0.78$, ε is the strain, $\Delta T = T - T_0$, where T is the current temperature and T_0 the temperature at the measurement start, and a_g is the linear temperature sensitivity factor. The strain is composed by the mechanical strain, ε_m, and the thermal strain, ε_T. α_{sp} is the coefficient of thermal expansion.

$$\varepsilon = \varepsilon_m + \varepsilon_T \tag{11}$$

$$\varepsilon_T = \alpha_{sp} \cdot \Delta T \tag{12}$$

Introducing (10) and (11) in the relation (9)

$$\frac{\Delta\lambda}{\lambda} = K\varepsilon_m + \left(K\alpha_{sp} + \alpha_g\right)\Delta T \tag{13}$$

The mechanical strain is

$$\varepsilon_m = \frac{1}{K}\frac{\Delta\lambda}{\lambda_0} - \left(\alpha_{sp} + \frac{\alpha_g}{K}\right)\Delta T \tag{14}$$

For an FBG only for temperature measurements, that means $\varepsilon_m = 0$, the temperature is given by

$$\Delta T = \frac{1}{K\alpha_{sp} + \alpha_g} \cdot \frac{\Delta\lambda}{\lambda_0} \tag{15}$$

To measure only the influence of the mechanical strain, a compensation procedure should be applied.

For a FEM numerical analysis, the case of a rectangular aluminum plate with dimensions of 250x20x0.2 mm is considered. Using the commercial software package PASTRAN/NASTRAN, the mode of the unbalanced deformation (strain) in the studied structure are computed. The results were compared with the analytical and experimental ones obtained in the laboratory. The material used is Al 2024 characterized by a Young modulus of 73100 MPa, and a density of 2780 kg/m3. The discretization is made using shell elements with an element size of approximately 5 mm.

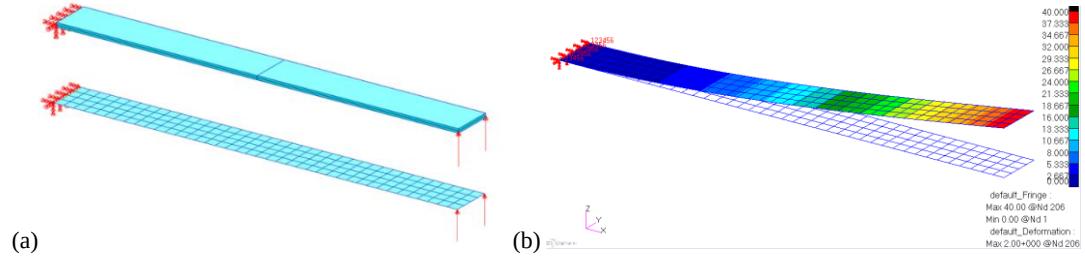

Fig. 3 (a) FEM model and the boundary conditions; (b) displacement variation

In Fig. 3 FEM model and the boundary conditions, which consist of blocking the all translations and rotations at one end and imposing a displacement at the other one, are presented. The imposed displacement starts at 2 mm and it is gradually increased with 2 mm until 40 mm.

3. EXPERIMENTAL TEST RIG

On a rectangular plate made from aluminium alloy EN AW-6060 AlMgSi, with 250 mm length, 20 mm width, and 2 mm thickness, an optical fiber was bonded, Fig. 4a. The bonding procedure is standard: surface degreasing with specific products, surface cleaning with abrasive sand paper, surface and fiber cleaning with reagents, adhesive applying, fiber positioning and pressing until the adhesive dries. The FBG area is fixed on the plate with fixing reagents. An electric gauge is applied near the optical sensor to compare the results.

The FBG sensor calibration setup is composed by an embedding device for the one end of the aluminum plate and also by the controlling mechanism of the free end of the plate, which has the role to create controlled, precisely displacements, measured with a displacement laser sensor, Fig. 4b. The model T90X-100D (http://www.manualpositioning.com/) ensures applications in precision motion control.

The software for movement control, data measurement and recording, and data analysis are part of the system configuration (Fig. 5).

(a) 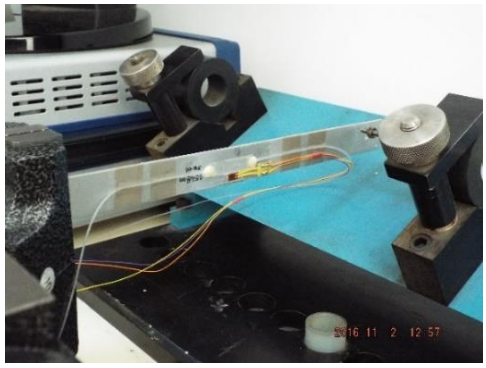 b) 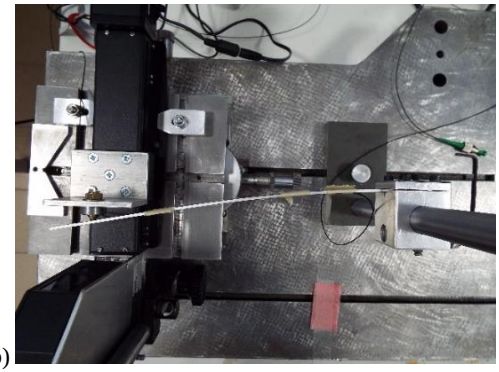

Fig. 4 (a) FBG optical sensor and the electric gauge bonded on the aluminium plate;
(b) experimental calibration set-up of the FBG optical sensor

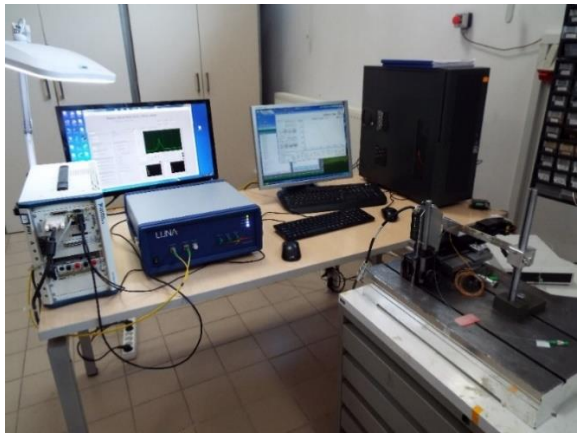

Fig. 5 Experimental test rig

In order to induce and measure the deformation in the aluminum plate, the system T90X-100D with digital display is used. It performs high precision linear controlled displacements. Fig. 4a shows a sequence on bending measurements. The optical fibre is bonded at 10 cm and the measurement point is fixed at 20 cm from the embedded end. Initially, the plate is unstrained and the movement slider is set at the origin point. Then, the system T90X-100D slider is gradually moved with a pre-set step.

4. RESULTS AND DISCUSSION

In a first stage of the measurement, the PH 1400 Phoenix tunable laser manufactured by Luna Inc. Is used, under PC control, to measure the spectrum of the FBG sensor used. Control is done on a USB bus that connects the two entities. The controller sets the lower limit and the upper limit of the wavelength range to be scanned by the PH 1400 device, the laser emission power, trigger type used as well as trigger thresholds, scanning speed and sampling rate, and then triggers the sweep.

After the entire range of set wavelengths has been scanned, the acquired data is sent to the controller where it is stored and then processed to be displayed graphically or saved in files for further processing. Figure 6 shows the repeatability of the measured data with Micron Optics OS 1100 sensor, 1548 nm.

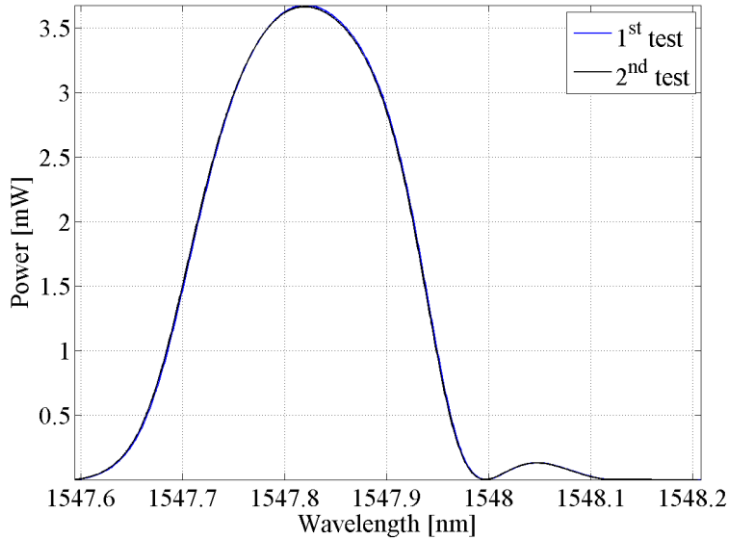

Fig. 6 The spectral feature of the FBG type OS 1100 Micron Optics for two tests

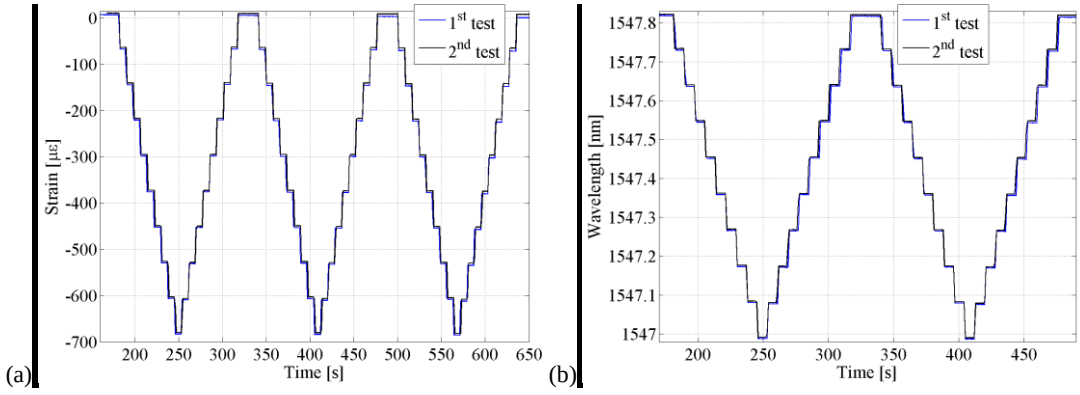

Fig. 7 Variation in time of strain (a) and of wavelength (b)

After determining the maximum, the bandwidth is defined as the range of wavelengths between the wavelengths corresponding to a 50% attenuation of the received power peak. Bandwidth is also known as FWHM (Full Width at Half Maximum).

The CW is then calculated, which is the midpoint between the wavelengths when the transmission factor is 50% of the specified minimum transmission, referred to as the Full Half Width (FWHM) width.

Fig. 7 shows the variation of the strain (unit deformation) and of the wavelength in time. At the initial moment the plate is free, so the FBG optical sensor is not exerted. Thus, the strain starts from scratch. Later, the cursor of the linear displacement device exerts a force on the aluminum plate, causing it to bend.

The cursor travel is 0.2 cm. Depending on how the plate in the demonstrator is positioned, the FBG sensor will perform a flexion motion, or a compression motion, so that the unitary deformation will be positive or negative.

It is noticeable that the FBG has a reasonable hysteresis in the return tests to the initial state, Fig. 8. The comparison of the strain analytical, numerical and experimental data indicates an accuracy of 1.49 at the hysteresis level.

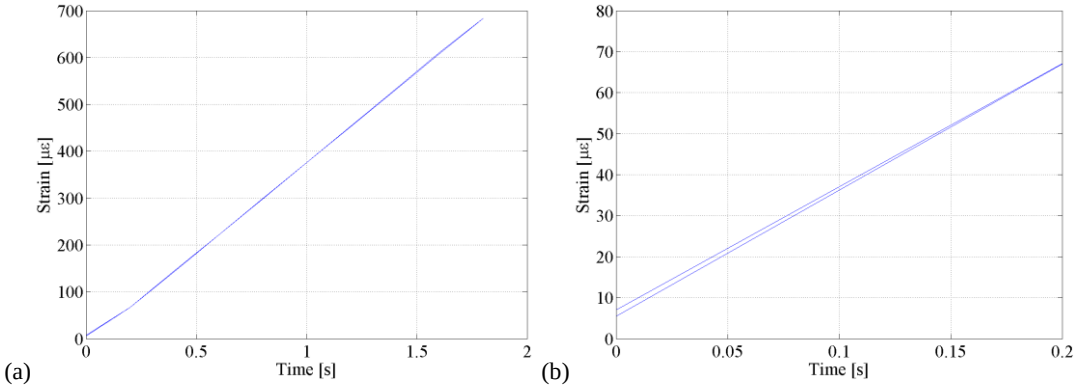

Fig. 8 Hysteresis curve: (a) across the full range; (B) zoom (difference 1.49 με)

Table 1. Experimental, analytic, and FEM results concerning strain induced by plate bending

displacement	*strain [με]**				
[cm]	*experimental***	*analytic*	*relative error[%]*	*FEM*	*relative error[%]*
0	0	0	0	0	0
0.2	76.221	75	1.60	75.89	0.43
0.4	153.448	150	2.25	151.8	1.07
0.6	229.571	225	1.99	227.7	0.81
0.8	305.475	300	1.79	303.6	0.61
1	381.604	375	1.73	379.4	0.58
1.2	458.054	450	1.76	455.3	0.60
1.4	533.951	525	1.68	531.2	0.52
1.6	609.404	600	1.54	607.1	0.38
1.8	685.711	675	1.56	683	0.40
2	762.818	750	1.68	758.9	0.51
2.2	839.25	825	1.70	834.8	0.53
2.4	916.03	900	1.75	910.7	0.58
2.6	992.638	975	1.78	986.5	0.62
2.8	1062.103	1050	1.14	1062	0.01

* the data varies with the temperature
**the average of more consecutive experiments

Fig. 9 shows the variation of the unit deformation with the maximum deflection given by the movement of the the system T90X-100D slider. As expected, the unit deformation varies linearly with the wavelength.

Graphs of experimental results are presented, but also of analytically calculated data, as well as given bt FEM numerical methods.

As can be seen in Table 1, experimentally obtained data are found around the analytically obtained values.

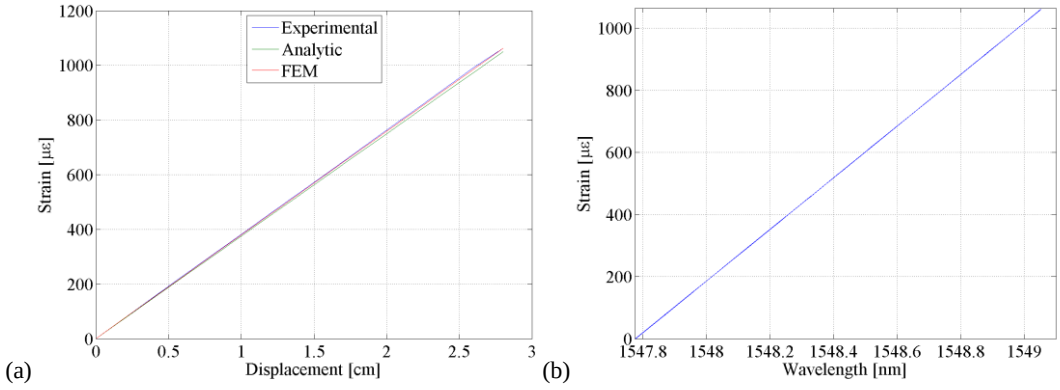

Fig. 9 (a) Variation of the strain with the maximum deflection (cursor movement);
(b) variation of the strain with wavelength

5. CONCLUSIONS

The small difference between the experimental, analytical and numerical values of the strain at the bending of the plate (Table 1) indicates the achievement within the project of a level of knowledge and competence necessary for later use of FBG sensors in the applicative researches involving the aerospace structures monitoring.

The results presented in the paper are only a small part of the results obtained within the project. Other measurements are related to temperature and acceleration sensors and FBG sensor behavior analysis under traction and compression conditions. It is important to mention that the research in this project continues the researches related to structures health monitoring based on of active piezo sensors [14]-[16].

ACKNOWLEDGEMENTS

The support from the Romanian Ministry of Research and Innovation-ANCS for the Project code PN 16 38 03 01 “Modern technologies for aerospace structures health monitoring”, in the framework of the NUCLEU Program, is thankfully acknowledged.

REFERENCES

[1] I. Mckenzie and N. Karafolas, *Fiber optic sensing in space structures: the experience of te European Space Agency*, in 17th International Conference on Optical Fibre Sensors, Bellingham, Washington, 2005.
[2] H. Guo, G. Xiao, N. Mrad and J. Yao, Fiber optic sensors for Structural Health Montioring of air platforms, *Sensors*, vol. **11**, pp. 3687-3705, 2011.
[3] I. Garcia, J. Zubia, G. Durana, G. Aldabaldetreku, M. A. Illarramendi and J. Villatorro, Optical fiber sensors for aircraft Structural Health Monitoring, *Sensors*, vol. **15**, pp. 15494-15519, 2015.
[4] S. J. Mihailov, Fiber Bragg Grating sensors for harsh environments, *Sensors*, vol. **12**, pp. 1898-1918, 2012.
[5] P. Ferdinand, *The evolution of optical fiber sensors technologies during the 35 last years and their applications in Structural Health Monitoring*, in 7th European Workshop on Structural Health Monitoring, La Cite, Nantes, France, 2014.
[6] W. J. Staszewski, C. Boller and G. R. Tomlinson, *Health Monitoring of Aerospace Structures. Smart Sensor Technologies and Signal Processing*, John Wiley & sons, Ltd, 2004.
[7] A. Guemes, *SHM technologies and applications in aricraft structures*, in 5th International Symposium on NDT in Aerospace, Singapore, 2013.
[8] A. Stancalie and G. Ilie, Experimental characterization of the optical fiber sensors, *UPB Sci. Bull., Series A*, vol. **78**, no. 1, pp. 299-308, 2016.

[9] H. M. Chan, A. R. Parker, A. Piazza and L. W. Richards, *Fiber-optic sensing system: overview, development and deployment in flight at NASA*, in Avionics and Vehicle Fiber-Optics and Photonics Conference, Santa Barbara, CA, USA, 2015.
[10] G. Wang, J. Zeng, H. Mu and D. Liang, Fiber Bragg Grating Sensor Network Optimization, *Photonic Sensors*, vol. **5**, no. 2, pp. 116-122, 2015.
[11] M. M. Filonenco-Borodici, S. M. Iziumov, B. A. Olisov, I. N. Cudriatev and L. I. Malghinov, *Curs de rezistenta materialelor, partea a II-a*, Ed. Tehnica, Bucuresti, 1952.
[12] A. Sommerfeld, *Mechanics of deformable bodies, vol II*, Academic Press, New York, 1950.
[13] D. C. Betz, *Application of optical fiber sensors for structural health monitoring*, Thesis, University of Sheffield, 2004.
[14] D. Enciu, I. Ursu, A. Toader, New results concerning SHM technology qualification for transfer on space vehicles, *Structural Control and Health Monitoring*, https://doi.org/10.1002/stc.1992, 2017.
[15] I. Ursu, D. Enciu, A. Toader, Towards structural health monitoring of space vechicles, *Aircraft Engineering and Aerospace Technology*, DOI: 10.1108/AEAT-07-2015-0173.R1, 2017.
[16] C. Rugina, A. Toader, V. Giurgiutiu, I. Ursu, The electromechanical impedance method for structural health monitoring of thin circular plates, *Proceedings of the Romanian Academy, Series A, Mathematics, Physics, Technical Sciences, Information Sciences*, vol. **15**, no. 3, pp. 272-282, 2014.